PAPER

Prelaunch spectral calibration of a carbon dioxide spectrometer

IOP Publishing Measurement Science and Technology
Meas. Sci. Technol. **28** (2017) 065801 (9pp) https://doi.org/10.1088/1361-6501/aa6507

Prelaunch spectral calibration of a carbon dioxide spectrometer

Zhigang Li, Chao Lin, Chengliang Li, Long Wang, Zhenhua Ji, Hao Xue, Yuefeng Wei, Chenghu Gong, Minghui Gao, Lei Liu, Zhiliang Gao and Yuquan Zheng

Changchun Institute of Optics, Fine Mechanics and Physics, Chinese Academy of Sciences, Changchun 130033, People's Republic of China

E-mail: lizhg@ciomp.ac.cn (Z Li) and zhengyq@sklao.ac.cn (Y Zheng)

Received 9 January 2017, revised 6 March 2017
Accepted for publication 7 March 2017
Published 12 April 2017

Abstract

The carbon dioxide spectrometer (CDS) on board the Chinese Carbon Dioxide Observation Satellite (TanSat) is a high spectral and spatial resolution grating spectrometer with three specific spectral bands dedicated to atmospheric CO_2 detection. The CDS's design and on-ground spectral calibration are presented in this paper. The instrument line shape functions and spectral dispersion were characterized using a tunable diode laser-based testing system for all spectral pixels of the CDS placed in a thermal vacuum chamber.

Keywords: spectral calibration, grating spectrometer, instrument line shape (ILS), spectral dispersion

(Some figures may appear in colour only in the online journal)

1. Introduction

The global mapping and change monitoring over time of concentrations of atmospheric carbon dioxide (CO_2), which is the most important anthropogenic greenhouse gas, are important tasks for studying Earth's climate changes. Ground-based and aircraft measurements are insufficient for achieving the resolution or coverage required to identify CO_2 sources and sinks over the globe. Space-based high resolution spectroscopic measurements of reflected sunlight in near-infrared CO_2 and O_2 bands for retrieving spatial variations in the column-averaged CO_2 dry air mole fraction (X_{CO_2}) can be used to improve the spatial and temporal sampling of CO_2 [1]. Coupled with atmospheric transport models, space-based remote sensing observations have provided an important and effective approach to addressing these issues and ameliorate the scientific community's understanding of the global carbon cycle. Several satellite-borne instruments, such as the European Space Agency (ESA) EnviSat Scanning Imaging Absorption SpectroMeter for Atmospheric CHartographY (SCIAMACHY), the Japanese GreenHouse Gases Observing Satellite (GOSAT), the Thermal and Near infrared Sensor for carbon Observation Fourier Transform Spectrometer (TANSO-FTS) and NASA Orbiting Carbon Observatory-2 (OCO-2) [2–10], were developed and applied for space-based observations to infer atmospheric CO_2 concentrations on regional scales. The carbon dioxide spectrometer (CDS), developed by the Changchun Institute of Optics, Fine Mechanics and Physics, Chinese Academy of Sciences, is a high spectral and spatial resolution grating spectrometer dedicated to CO_2 detection by measuring reflected sunlight in three narrow bands including near-infrared weak and strong CO_2 bands around 1.61 μm and 2.06 μm, respectively, with a spectral resolving power of about 12 000 and a molecular oxygen (O_2) A-band around 0.76 μm with a spectral resolving power of about 19 000. The CDS is a main payload instrument onboard the Chinese Carbon Dioxide Observation Satellite (TanSat) [11, 12] dedicated to CO_2 detection and monitoring in a sun-synchronous orbit, launched on 22 December 2016. The CDS is designed to be similar to OCO-2 in band selection, but different in instrument characterization. Nadir, glint and target observation modes will be operated on the satellite to collect data for specific science applications. The footprint size is approximately 2 km $\times$ 2 km and the swath is about 20 km wide at nadir. Observation data will be received by a ground segment to implement X_{CO_2} retrievals and perform data validation by means of ground-based CO_2 monitoring.

Table 1. Comparison between the target specifications and the achieved prelaunch testing results of the CDS.

Parameter	Target performance	Prelaunch testing results
Spectral ranges	O_2 A-band: 758–778 nm Weak CO_2 band: 1594–1624 nm Strong CO_2 band: 2041–2081 nm	O_2 A-band: 757.382–778.093 nm Weak CO_2 band: 1593.973–1623.842 nm Strong CO_2 band: 2040.540–2080.498 nm
Spectral resolution	O_2 A-band: 0.033–0.047 nm Weak CO_2 band: 0.12–0.142 nm Strong CO_2 band: 0.16–0.182 nm	O_2 A-band: 0.0392–0.0424 nm Weak CO_2 band: 0.123–0.128 nm Strong CO_2 band: 0.157–0.168 nm
Signal to noise ratio	O_2 A-band: 360:1 (at 5.8×10^{19} photons/s/m^2/sr/μm) Weak CO_2 band: 250:1 (at 2.1×10^{19} photons/s/m^2/sr/μm) Strong CO_2 band: 180:1 (at 1.1×10^{19} photons/s/m^2/sr/μm)	Average SNR O_2 A-band: 455:1 (at 5.8×10^{19} photons/s/m^2/sr/μm) Weak CO_2 band: 260:1 (at 2.1×10^{19} photons/s/m^2/sr/μm) Strong CO_2 band: 185:1 (at 1.1×10^{19} photons/s/m^2/sr/μm)

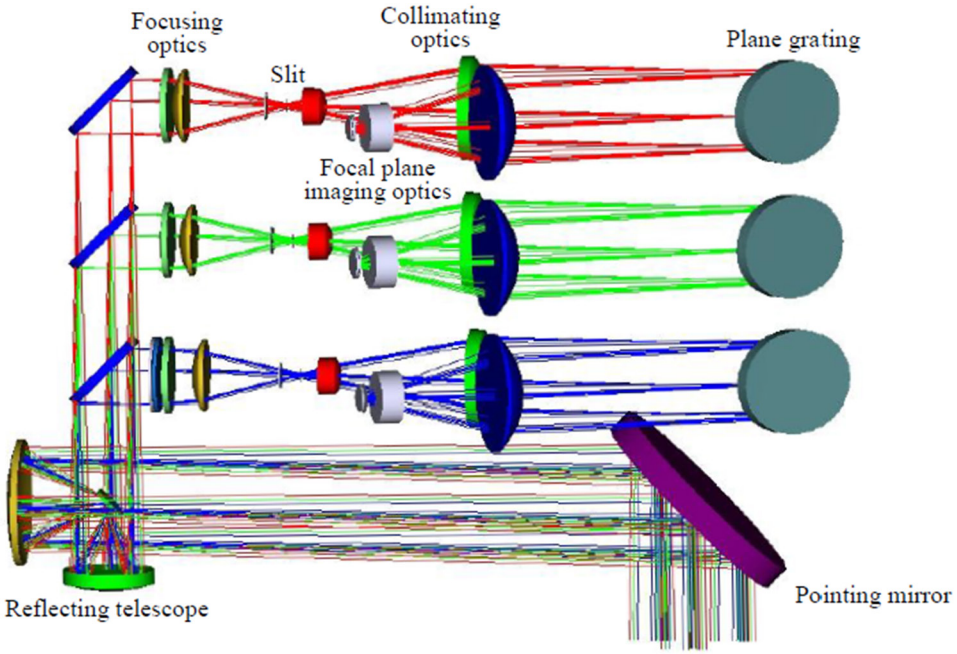

Figure 1. Schematic layout of the CDS optical system.

The radiometric and spectral calibrations of the CDS are performed before launch. A comparison of the target specifications and the prelaunch testing results for three important CDS instrument parameters is given in table 1. The CDS radiometric calibration, including characterizations of the instrument's absolute response and signal-to-noise ratio (SNR), will be described in a future paper. This paper concentrates on the prelaunch spectral calibration. A brief overview of the CDS instrument is described first. The results of prelaunch spectral calibration of the CDS instrument are presented in this paper. Tunable diode laser-based ILS and spectral dispersion with respect to each spectral pixel on the CDS's three imaging arrays were derived from this on-ground spectral calibration.

2. Description of the CDS

The CDS instrument, which includes three grating spectrometers that respectively correspond to three different spectral bands, is primarily composed of a pointing mirror, a common reflecting afocal telescope, beamsplitters, focusing systems, slits, collimating lenses, plane gratings and focal plane imaging systems. An optical schematic of the CDS is shown in figure 1. The pointing mirror, mounted on a 1D rotation mechanism, is a specially designed optical element with a double-sided function: the front side was designed and processed to be a mirror to reflect the incident light to the telescope, and the back side was designed and prepared by a process of physical grinding and chemical etching to be a reflecting diffuser for onboard instrument calibration. The optical design of the reflecting telescope is based on a coaxial double parabolic crossed afocal optical system with a beam contraction ratio of 3:2. The corresponding polarizer is placed in front of the slit of each spectrometer. The reflected optical radiation from the foreoptics system reaches the entrance slits of three spectrometers after being split, converged and then polarized, respectively. In each spectrometer, the light from the slit is collimated and directed to a plane grating. The image of the slit is formed on the focal plane detector surface after diffracted light passes through the imaging optical system.

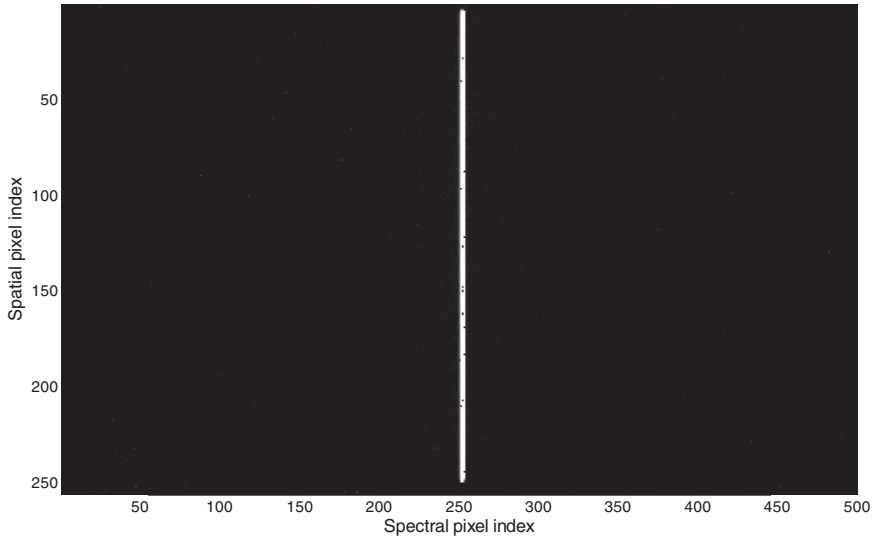

Figure 2. An image of the slit on the array detector of the 1610 nm band spectrometer.

The arrangement order of the three spectrometers, using three specific designed holographic plane gratings in different bands, is from the O_2 A-band (758 nm–778 nm), to the weak CO_2 band (1594 nm–1624 nm) and then the strong CO_2 band (2041 nm–2081 nm). The substrate materials of the two dichroic beamsplitters with different specially designed coatings are fused silica. The reflectivity of one beamsplitter is about 0.98 over the O_2 A-band, and the transmittance is about 0.98 over two CO_2 bands. The reflectivity of the other beamsplitter is about 0.99 over the weak CO_2 band and the transmittance is about 0.98 over the strong CO_2 band. A folding mirror was used instead of a beamsplitter for the last strong CO_2 band. The spectral dispersion of each spectrometer was determined mainly by holographic plane grating used for each measured spectral band. The lengths of three slits are approximately 8 mm, 7 mm, 7 mm and the widths are approximately 28 μm, 38 μm and 39 μm in turn. To reduce the effect of stray light, a narrow band isolation filter is placed between the beamsplitter and the condenser lens for the O_2 A-band, and placed in front of the detectors for the weak and strong CO_2 bands. A slightly curved entrance slit is used for each spectrometer to compensate for optical aberrations (and to correct the 'smile effect'), which in turn makes the image straight on the focal plane. The determination of the entrance slit curvature is based on the result from careful optical design for each spectrometer. As an illustration, an image of the slit on the array detector of the 1610 nm band spectrometer from a tunable diode laser source operated at a laser wavelength close to 1609.5 nm is shown in figure 2. The black spots in the slit image are caused by bad pixels. The bad pixels were identified by analysing dark current and radiometric response data obtained from prelaunch testing in a thermal vacuum chamber.

Since an increase in the area of the detector can effectively improve the SNR for an optical system with a fixed relative aperture, the detector pixel merging method is employed in the CDS. In the spatial dimension, a certain number of detector pixels are combined as a pixel to meet the ground resolution requirement of 2 km $\times$ 2 km. The charge-coupled device (CCD) detector (e2v CCD55-30) used in the O_2 A-band spectrometer was a 1252 $\times$ 1152 array with the size of single pixel being 22.5μm $\times$ 22.5μm. Only 1242 $\times$ 288 pixels among this array detector were actually used for measurements, and 1242 pixels were used in the spectral dimension. In the spatial dimension, 32 pixels were combined into a single pixel, which is equivalent to a spectral detection element size of 22.5 μm $\times$ 720 μm, i.e. the O_2 A-band spectrometer had nine spatial footprints and 1242 spectral channels in each footprint. Two CO_2-band spectrometers were configured with two identical 500 $\times$ 256 array mercury cadmium telluride (MCT) detectors (Sofradir Neptune SW), which have a single pixel size of 30μm $\times$ 30μm. The operating temperature can be cooled to 150 K with an active cooling system. Only 216 pixels were used out of the 256 in the spatial dimension and 500 pixels were used in the spectral dimension. In the spatial dimension, 24 pixels were combined into one pixel, which is equivalent to a spectral detection element size of 30 μm $\times$ 720 μm, i.e. the CO_2 band spectrometers had nine spatial footprints and 500 spectral channels in an individual footprint. The straight slit images on the array detector of each spectrometer are also beneficial for combining pixels with consistent centroid wavelength response in the spatial dimension to increase the SNR. The fixed frame rate of detector sampling was approximately 3.3 Hz and the integration time was approximately 293 ms.

The focal length of the spectrometer system and entrance slit size in the optical design were determined by the detector size, field of view and minimum spectral sampling interval. The field of view for each spectral detection pixel in three spectrometers is 2 km $\times$ 2 km. There are about two detector element spectral samplings within a full width at half maximum (FWHM) in each band of the CDS.

Before spectral calibration, bad pixel screenings of the area array detectors were performed to construct an onboard map, and the outputs of the bad pixels were set to zero during the measurements to remove their effects from calibration data processing.

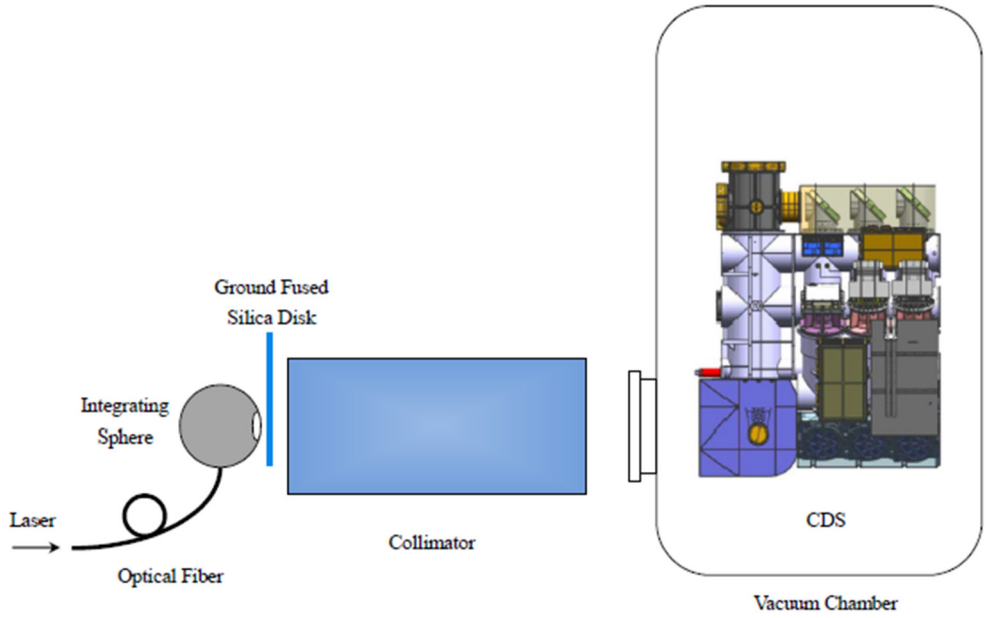

Figure 3. Schematic diagram of the experimental setup for CDS spectral calibration.

3. Spectral calibration

The targeted objective of the CDS spectral calibration is to measure the spectral dispersion and the ILS function of each detector element (the total number is 20178) among each of nine individual footprints in all three bands. The shape of the CDS ILS function is determined by the slit width, pixel pitch, optical aberrations, diffraction, detector crosstalk and stray light [8].

The CDS was placed in a thermal vacuum chamber, which was maintained in vacuum of the order of 10^{-3} hPa during the spectral calibration. We utilized three tunable diode lasers to scan each spectral range of three bands, respectively, to gauge the characterization of the ILS and the spectral dispersion.

Since averaging over data of payload image frames could improve the SNR, a total of 50 detector frame image data were collected with an acquisition time of 15 s, with regard to each laser wavelength scan during the spectral calibration measurements. An automation software program was used for setting the laser wavelength, awaiting laser wavelength and intensity stabilization and recording data. The wavelength accuracy from the laser wavelength meter was determined by the stabilities of the tunable laser and the laser wavelength meter. Two laser wavelength meters which covered different wavelength ranges were used for three tunable laser measurements, one (Bristol 621B-NIR) was used for the 760 nm and 1610 nm bands, another (Bristol 621B-IR) was used for the 2060 nm band. The absolute accuracy and repeatability of the two laser wavelength meters are ±0.75 ppm and ±0.1 ppm, respectively. After the test, the laser output wavelength stabilities of tunable diode lasers (for 760 nm, 1610 nm, and 2060 nm bands) were better than 0.2 pm, 0.6 pm and 0.4 pm, respectively, within each 15 s period.

The schematic of the spectral calibration device is shown in the figure 3. After passing through optical fibers with the beam splitting ratio of 9:1, 760 nm and 1610 nm band lasers were introduced to the integrating sphere, and 10% of the power was sent into the laser wavelength meter. For the 2060 nm band, the laser was introduced into the integrating sphere after sending reflected partial light to the wavelength meter. The method involving a tunable diode laser, integrating sphere and collimator was applied in CDS ILS tests. Three tunable diode lasers were used as light sources. Part of the laser was introduced to the wavelength meter for simultaneous laser wavelength and power monitoring. Another component of the laser was coupled by optical fiber into a 2 inch diameter integrating sphere with a Spectralon coating. The exit port of the integrating sphere was placed at the focal plane of collimator with a focus length of 250 mm so the CDS instrument in the chamber could be illuminated by uniform and collimated laser radiation through a window to conduct spectral calibration. In addition, because the laser speckle phenomenon caused by the laser radiation spatial coherence increases the fluctuation of the image data, a spinning ground fused silica disk was settled between the exit port of the integrating sphere and the entrance of collimator to suppress the speckle effects. The wavelength scan ranges of the three tunable diode lasers used for ILS tests were approximately 758.2–777.2 nm, 1592.8–1624 nm and 2040.3–2076.7 nm. The wavelength scan step sizes chosen for three laser measurements were 0.005 nm, 0.015 nm and 0.02 nm, independently. However, for instance, in a section of the longer wavelength region of the strong CO_2 band (2041 nm–2081 nm), the laser wavelength was not covered. The maximum wavelength that was covered was approximately 2076.7 nm. In the absence of a laser wavelength scan, an extrapolation method was used to deal with the calibration data.

The CDS detector responses to different wavelength laser radiation were collected after scanning tunable diode lasers. After removing the background noise, inputting laser optical power correction and Gaussian fitting, the centroid wavelength λ_{cen} of each spectral pixel covered by the laser

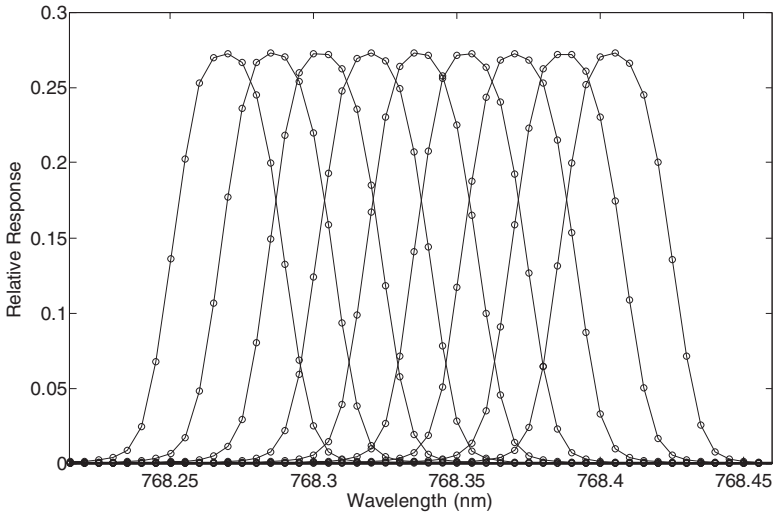

Figure 4. Relative response of the nine neighboring spectral pixels to tunable diode laser scans in the O_2 A-band.

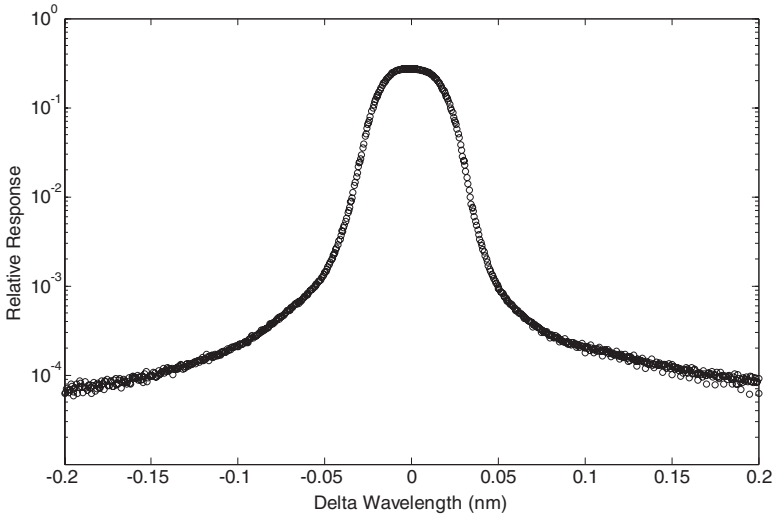

Figure 5. A combined centered response data set of nine neighboring spectral pixels.

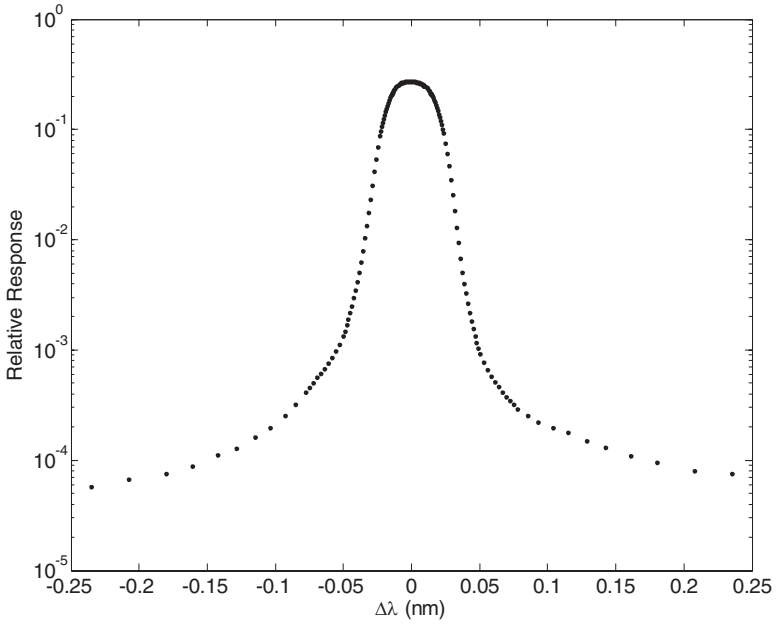

Figure 6. 200 $\Delta\lambda$ point data set of initial ILS for spectral pixel index 605 in fifth footprint of O2 A-band.

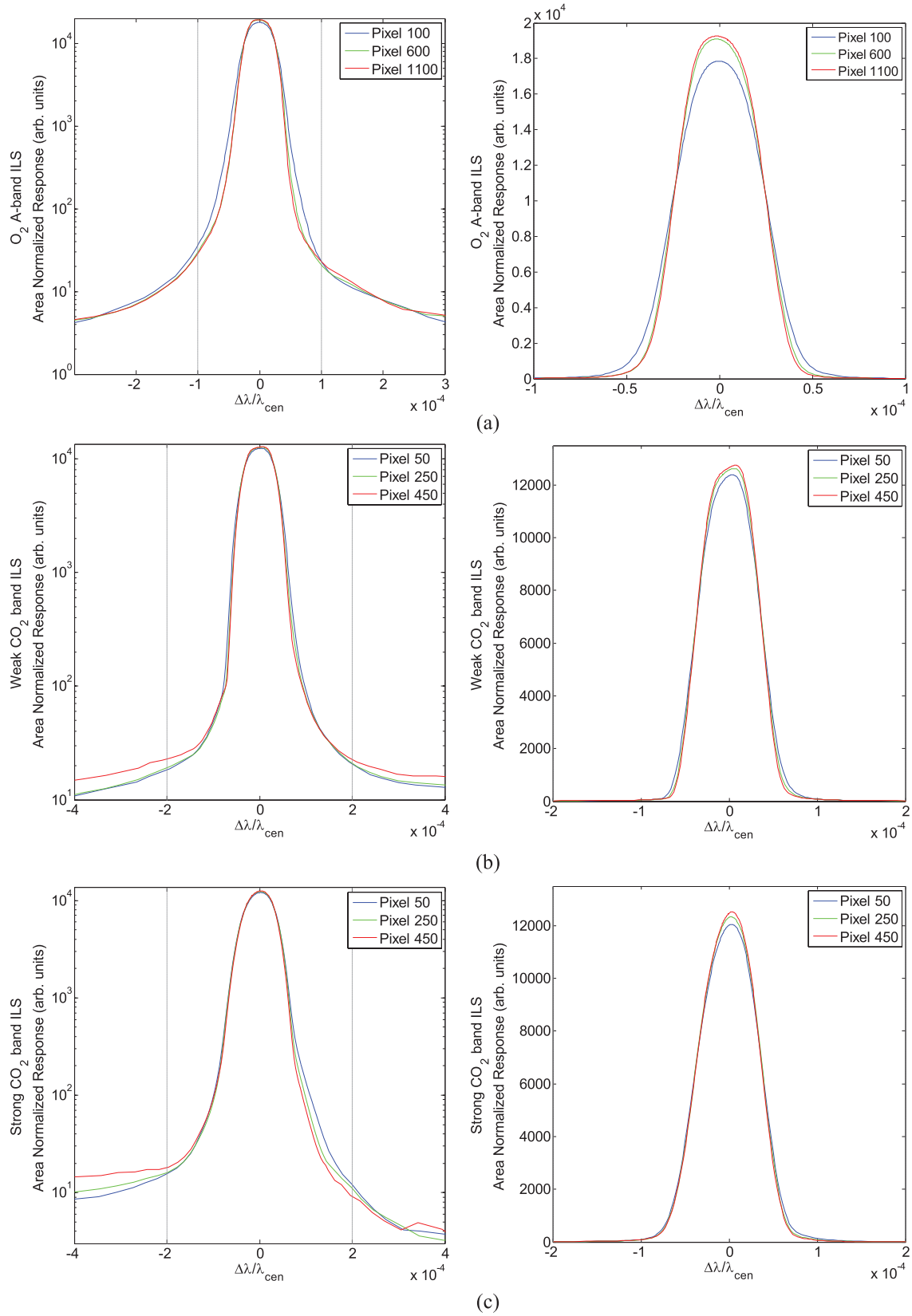

Figure 7. Typical derived ILS profiles for three bands at different spectral pixel indexes. (a) O_2 A-band ILS (b) weak CO_2 band ILS (c) strong CO_2 band ILS left: semilog plot of the ILS. Right: linear plot of the ILS corresponding to the section delimited by the dashed lines in the left plot.

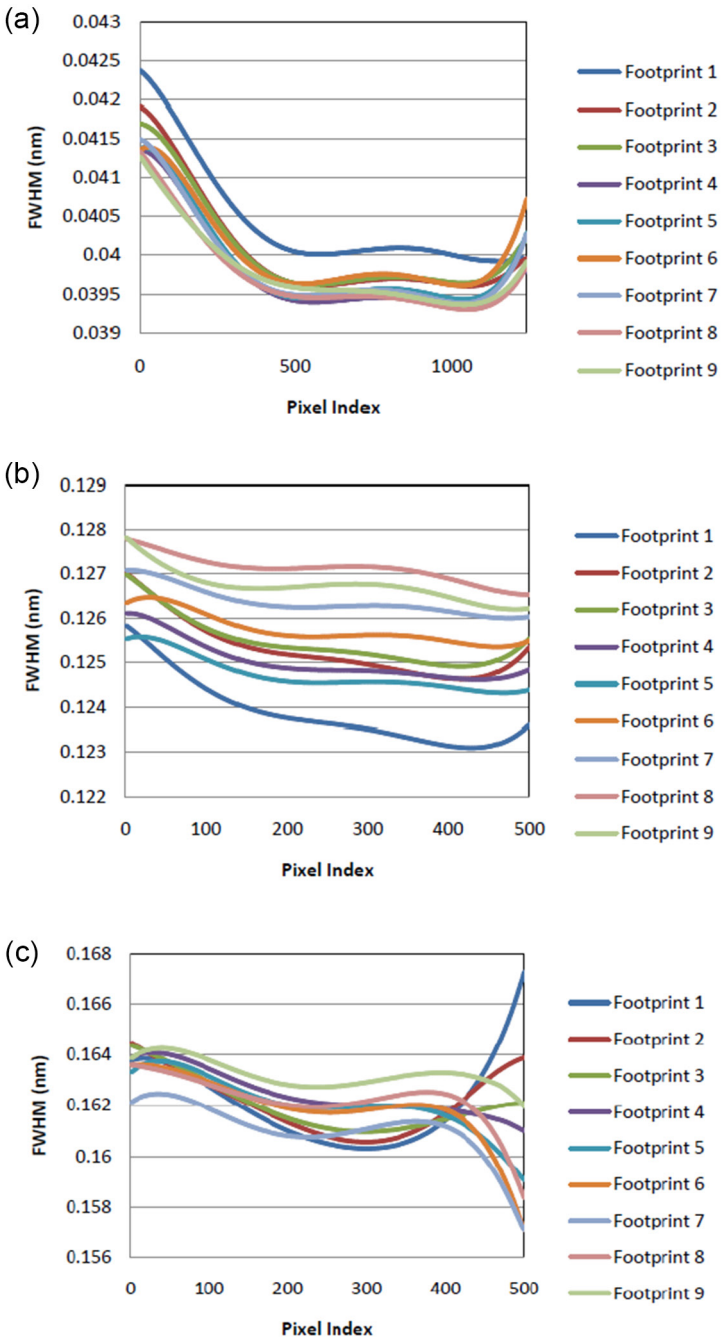

Figure 8. FWHM values of spectral pixels in each band. (a) O_2 A-band (b) weak CO_2 band (c) strong CO_2 band.

scan ranges was yielded. Figure 4 shows the representative relative response from nine adjacent spectral pixels to laser scans, with pixel index numbers from 601 to 609 in footprint 5 of the 760 nm band spectrometer. Assuming the adjacent spectral pixels had nearly identical ILSs, the combination of calibrated responses from a group of adjacent spectral pixels (with each centroid wavelength as center) would enrich the data for a better ILS function fitting of the center spectral pixel. Compacted spectral sampling can be acquired when the response from neighboring pixels is combined. A combined single data set from the above nine relative responses for spectral pixel 605 (in footprint 5 of the 760 nm band spectrometer) is shown in figure 5. Because conventional line-shape functions are incapable of fitting the shapes well enough for accurate X_{CO_2} retrievals [10], after forming an ILS data set for each spectral pixel as a function of $\Delta\lambda = \lambda - \lambda_{cen}$, 200 fixed delta wavelength coordinates were chosen with sampling that was dense in the middle but sparse on both sides according to different sensitivity to small variations in the ± 0.235 nm, ± 0.7 nm and ± 0.925 nm width range corresponding to 760 nm, 1610 nm and 2060 nm bands, respectively, for the next step process of regional fitting. Thereby, tabular ILS functions can be used for interpolation. Subsequently, we selected 21 data points in the closest domain to each fixed wavelength abscissa to make a cubic polynomial fit, and then the longitudinal coordinate value corresponding to this fixed abscissa

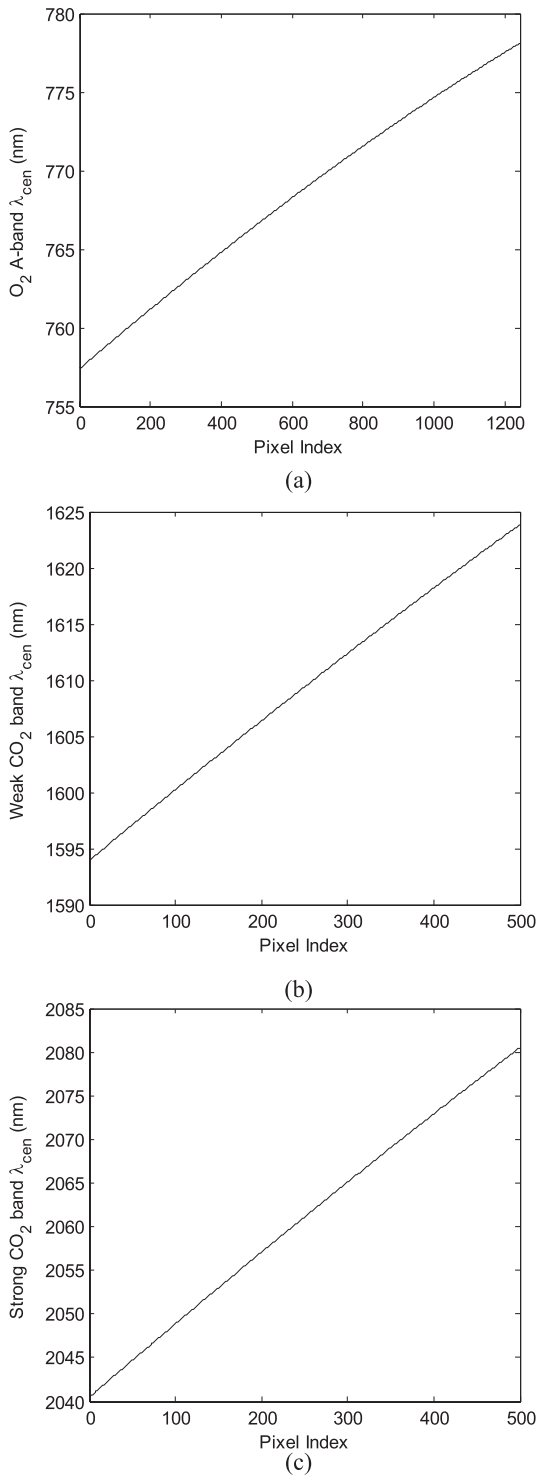

Figure 9. Typical sixth-order polynomial fits to spectral dispersion for each footprint 5 in three bands as a function of spectral pixel index. (a) O_2 A-band (b) weak CO_2 band (c) strong CO_2 band.

was carried out via interpolation. A representative ILS profile, which consisted of 200 $\Delta\lambda$ points (the pixel index is 605 in the fifth footprint of the 760 nm band spectrometer) is shown in figure 6.

In accordance with the assumption for each spectral band that each spectral pixel ILS as a function of $\Delta\lambda$

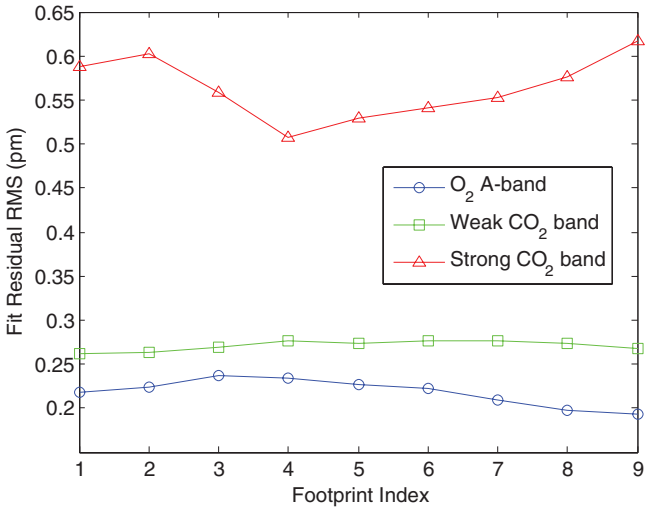

Figure 10. The RMS values of fit residuals for nine spatial footprints in each of three bands.

varied smoothly along with pixel index, each of the area-normalized 200 ILS points of a spectral pixel were fitted using a polynomial and interpolated as a function of spectral pixel index to produce a laser-based ILS data set. A fifth-order fit was mainly used, especially for locations near the ILS core. A second-order fit was used for some locations in the ILS wings depending on the actual situations of pixel relative response on the spectral pixel index. Shown in figure 7 are the derived area-normalized ILS profiles for the fifth spatial footprint for three CDS bands at three different spectral pixel indexes. Asymmetry was found in CO_2 band ILS profiles in particular.

The FWHM values of the spectral pixels shown in figure 8 are within the range of 0.0392–0.0424 nm, 0.123–0.128 nm and 0.157–0.168 nm for the O_2 A-, weak CO_2 and strong CO_2 bands, respectively. This satisfies the CDS instrument spectral resolution requirements.

Interpolation and extrapolation were separately performed for within and outside the laser scan ranges by fitting a sixth-order polynomial to the Gaussian-fitted centroid wavelength as a function of pixel index to determine the spectral dispersion for each of nine footprints in three spectral bands of the CDS instrument. Figure 9 shows three fitted spectral dispersion curves of three bands for footprint 5 as a function of spectral pixel index. The RMS values of fit residuals for nine spatial footprints in each of three bands are shown in figure 10. The maximum fit residual RMS values are approximately 0.236 pm, 0.277 pm and 0.617 pm, respectively, in three bands. The overall RMS errors of nine footprints are worst in the strong CO_2 band and are best in the O_2 A-band. The maximum-to-minimum differences of centroid wavelengths between nine spatial footprints for each spectral pixel in three bands are shown in figure 11. The maximum differences are approximately 0.017 nm, 0.016 nm and 0.021 pm independently for three bands. From the results of spectral dispersion, the spectral ranges of CDS three spectrometers are 757.382–778.093 nm, 1593.973–1623.842 nm and 2040.540–2080.498 nm separately.

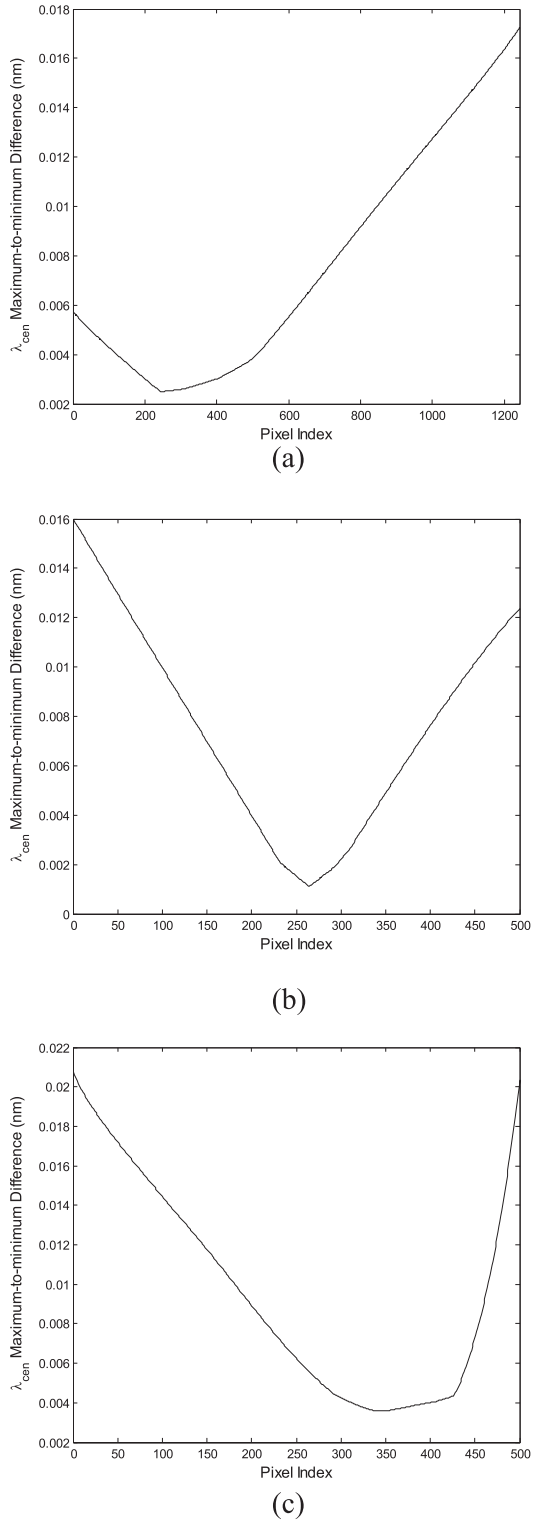

Figure 11. The maximum to minimum centroid wavelength differences between nine spatial footprints for three bands as a function of spectral pixel index. (a) O_2 A-band (b) weak CO_2 band (c) strong CO_2 band.

4. Conclusion

This paper has depicted the instrument features, performance, as well as the prelaunch on-ground spectral calibration of the CDS. The calibration data was obtained by illumination of the CDS entrance port through a vacuum chamber window with a dedicated on-ground testing system equipped with three tunable diode laser sources during the prelaunch spectral calibration. Spectral dispersion equations and ILS functions of all spectral pixels were tested and derived from tunable diode laser fine step scans for the prelaunch CDS spectral calibration. Further validation and refinement of ILS profiles and spectral dispersion equations can be implemented after the launch using in-orbit calibration measurement data. The CDS will be expected to meet its principal mission of globally identifying CO_2 sources and sinks at a required spectral resolution and spectral calibration accuracy with the on-ground laser-based spectral calibration results.

Acknowledgments

This research described in this paper was performed with support from the National High-tech R&D Program of China (2011AA12A102).

References

[1] Crisp D *et al* 2004 The Orbiting Carbon Observatory (OCO) mission *Adv. Space Res.* **34** 700–9
[2] Bovensmann H, Burrows J P, Buchwitz M, Frerick J, Noel S and Rozanov V V 1999 SCIAMACHY: mission objectives and measurement modes *J. Atmos. Sci.* **56** 127–50
[3] Schneising O, Buchwitz M, Reuter M, Heymann J, Bovensmann H and Burrows J P 2011 Long-term analysis of carbon dioxide and methane column-averaged mole fractions retrieved from SCIAMACHY *Atmos. Chem. Phys.* **11** 2863–80
[4] Kuze A, Suto H, Nakajima M and Hamazaki T 2009 Thermal and near infrared sensor for carbon observation Fourier-transform spectrometer on the greenhouse gases observing satellite for greenhouse gases monitoring *Appl. Opt.* **48** 6716–33
[5] Sakuma F, Bruegge C J, Rider D, Brown D, Geier S, Kawakami S and Kuze A 2010 OCO/GOSAT preflight cross-calibration experiment *IEEE Trans. Geosci. Remote Sens.* **48** 585–99
[6] Haring R, Pollock R, Sutin B and Crisp D 2005 Current development status of the Orbiting Carbon Observatory instrument optical design *Proc. SPIE* **5883** 58830C
[7] O'Dell C W, Day J O, Pollock R, Bruegge C J, O'Brien D M, Castano R, Tkatcheva I, Miller C E and Crisp D 2011 Preflight radiometric calibration of the Orbiting Carbon Observatory *IEEE Trans. Geosci. Remote Sens.* **49** 2438–47
[8] Day J O, O'Dell C W, Pollock R, Bruegge C J, Rider D, Crisp D and Miller C E 2011 Preflight spectral calibration of the Orbiting Carbon Observatory *IEEE Trans. Geosci. Remote Sens.* **49** 2793–801
[9] Basilio R R, Pollock H R and Hunyadi-Lay S L 2014 OCO-2 (Orbiting Carbon Observatory-2) mission operations planning and initial operations experiences *Proc. SPIE* **9241** 924105
[10] Frankenberg C *et al* 2015 The Orbiting Carbon Observatory (OCO-2): spectrometer performance evaluation using pre-launch direct sun measurements *Atmos. Meas. Tech.* **8** 301–13
[11] Liu Y, Yang D and Cai Z 2013 A retrieval algorithm for TanSat X_{CO_2} observation: retrieval experiments using GOSAT data *Chin. Sci. Bull.* **58** 1520–3
[12] Liu Y, Cai Z, Yang D, Zheng Y, Duan M and Lü D 2014 Effects of spectral sampling rate and range of CO_2 absorption bands on X_{CO_2} retrieval from TanSat hyperspectral spectrometer *Chin. Sci. Bull.* **59** 1485–91